IMA Journal of Mathematical Control and Information (2020) **37**, 1572–1590
doi:10.1093/imamci/dnaa025
Advance Access publication on 12 October 2020

Passivity-based control of islanded microgrids with unknown power loads

Sofía Avila-Becerril and Gerardo Espinosa-Pérez*
Facultad de Ingeniería, Universidad Nacional Autónoma de México. Av Universidad 3000, CDMX, 04510, México
*Corresponding author. Email: gerardoe@unam.mx

Oscar Danilo Montoya
Laboratorio Inteligente de Energía, Universidad Tecnológica de Bolívar, km 1 vía Turbaco, Cartagena 131001, Colombia. Facultad de Ingeniería, Universidad Distrital Francisco José de Caldas, Carrera 7, Bogotá D.C. 11021, Colombia

and

Alejandro Garces
Department of Electric Power Engineering, Universidad Tecnológica de Pereira. AA: 97, 660003 Pereira, Colombia

[Received on 15 November 2019; revised on 4 August 2020; accepted on 1 September 2020]

In this paper, the control problem of microgrids (MGs)operating in islanded mode is approached from a passivity-based control perspective. A control scheme is proposed that, relying only on local measurements for the power converters included in the network representation, achieves both voltage regulation and power balance in the network through the generation of grid-forming and grid-following nodes. From the mathematical perspective, the importance of the contribution lies in the feature that, exploiting a port-controlled Hamiltonian representation of the MG, the closed-loop system's stability properties are formally proved using arguments from the theory of non-linear dynamical systems. Fundamental for this achievement is the decomposition of the system into subsystems that require a control law and another whose variables can evolve in a free way. From the practical viewpoint, the advantage of the proposed controller lies in the feature that the power demanded by the loads is satisfied without neither computing its specific value nor solving the non-linear algebraic equations given by the power flow, avoiding the computational burden associated with this task. The usefulness of the scheme is illustrated via a numerical simulation that includes practical considerations.

Keywords: microgrids; islanded operation mode; passivity-based control; Hamiltonian systems.

1. Introduction

A microgrid (MG) is an electrical network that interconnects loads with distributed energy resources (DERs), the latter mainly given by renewable energy sources like photovoltaic (PV), eolic and battery among others. The mixed nature of DERs imposes the necessity of including power converters to homogenize the generated electrical energy and make it compatible with the load requirements. MGs can operate connected to the main grid, in grid-connected mode, or in autonomous operation, in islanded mode. Regardless of the operation mode, their objective is to satisfy the power demanded by the loads ensuring, at the same time, that the bus voltages remain within allowed values (Gu *et al.*, 2014; Han *et al.*, 2015; Shuai *et al.*, 2016; Bidram *et al.*, 2017; Rojas & Rousan, 2017).

Due to the structure described above, MGs' control problem imposes additional challenges concerning the usually found in conventional power systems. One that is fundamental is related to the absence of rotating masses, a condition that drastically increases the system sensitive to the appearance of sudden and fast changes in the operating conditions (Gu *et al.*, 2014; Arani *et al.*, 2017; Tuffner *et al.*, 2018). This situation generates a two-fold complication: the necessity of including local (primary) high-performance controllers for the power converters to achieve the operation objective (Bouzid *et al.*, 2015; Han *et al.*, 2015) and the imperative requirement of including the influence of these electronic devices in the dynamic analysis of the whole network (Pogaku *et al.*, 2007).

The complexity involved in both the controller design and the dynamic analysis problems for MGs lies in the fact that the models for these systems are given by a set of non-linear differential equations subject to a set of non-linear algebraic equations. The former due to the topological structure of the non-linear electrical circuits used to represent the power converters and loads connected to the network, while the latter coming from the mathematical representation of the power exchanged among the different elements that participate in the network (the well-known load flow equations).

In order to deal with the problematics described above, the usual approach to design control schemes is to consider a hierarchical structure. The basic level is dedicated to guarantee a stable power converters operation, in the sense that voltages and currents exhibit a bounded behaviour, to later on consider a second control level whose purpose is to determine the specific value for the variables associated to the converters that correspond to a prescribed power balance. This two-step design is endowed with additional desired features like the avoidance of requiring information of the whole network for a local controller operation and, especially in the islanded operation mode, that some converters generate a voltage reference (grid-forming operation) while others provide a fixed amount of power (grid-following operation).

Diverse solutions to the control problem above can be found in the literature standing out the use of model-free algorithms, mostly PI-based structures, for the power converters operation. Despite the widely recognized advantages of these schemes, their main drawback lies in the lack of a formal analysis of their stability properties, leading to a time-consuming tuning and the eventual generation of instabilities (Bouzid *et al.*, 2015). Some efforts have been reported to deal with these problems like the (decentralized) model predictive control, but besides the high order required for the control scheme, the stability analysis problem is not completely solved since the design is based on a linearized representation of the system (Jayachandran & Ravi, 2019). On the other hand, two main approaches can be identified to deal with the power balance objective. The first corresponds to the numerical solution of the load flow equations, while the second corresponds to the proposition of what are known as droop-based (also model-free) schemes. Although the numerical alternative is well dominated, its disadvantage lies in the computational burden and its offline nature (Agundis-Tinajero *et al.*, 2019). Concerning the study of droop-based strategies, the stability analysis of these kinds of schemes has been solved to a very large extent including a Hamiltonian approach (Schiffer *et al.*, 2014), the interpretation of the system operation from a multiagent perspective (Simpson-Porco *et al.*, 2013), the inclusion of economic constraints (Stegink *et al.*, 2016) and the use of input-to-state stability arguments (Konstantopoulos *et al.*, 2015). However, all these results consider only the dynamic behaviour of power variables disregarding the power converters' presence and its associated phenomena without approaching the dynamic analysis of the whole network.

In this paper, a solution to the control problem of MGs is presented exhibiting two main features: a complete dynamical model for the network is considered, including the influence of detailed non-linear models for the power converters, and the stability properties induced by the proposed controller are formally proved without disregarding any element of the whole network. Besides, the contribution

enjoys the properties that its implementation relies only on the measurement of local variables, guarantees the generation of both grid-forming and grid-following nodes and the power network balance is achieved without the specific computation of the power demanded by the loads, avoiding the use of neither numerical methods nor droop-based schemes.

The key characteristic of the contribution design methodology is the representation of all the elements that compose an MG (voltage-fed and current-fed converters, the network topology and the loads) in terms of the interconnection of port-controlled Hamiltonian (PCH) systems (van der Schaft & Maschke, 2013), since under this context,

- a passivity-based controller (PBC) for each one of the DERs was designed to ensure the convergence of their voltage and current to bounded prescribed values and
- the system could be decomposed into subsystems that required a control law to reach a proper behaviour and a subsystem whose variables can evolve in a free way as long as they describe a bounded behaviour. This decomposition facilitated, complementing the PBC design, the use of cascaded systems theory to develop the network stability analysis.

The last feature of the proposed controller scheme concerns the way how the power balance objective was approached. In this sense, exploiting the identified decomposition of the system, it was proved that ensuring the grid-following nodes generate the maximum amount of available power and assuming that the grid-forming nodes are able to complement the demand of the loads, the behaviour of network variables naturally converge to the required power balance, i.e., it is not required to compute the loads' power demand explicitly.

The results presented in this contribution follows the ideas developed in Avila-Becerril *et al.* (2019) and Avila-Becerril & Espinosa-Pérez (2020) where different approaches have been proposed to solve the MG control problem. In particular, it is an extended and improved version of Avila-Becerril *et al.* (2018) in the sense that for both voltage-fed and current-fed converters, it is possible to impose active and reactive power profiles; besides, the stability properties of the whole closed-loop system are proved in a clear, complete and formal way by exploiting cascaded systems theory. On the other hand, the necessity to assume that the loads satisfy a passivity property is still present in the current state of the research work.

The rest of the paper is organized as follows. In Section 2, the model of the MG is presented. Section 3 introduces the controller used to stabilize the network, while the procedure to satisfy the power demanded by the loads is presented in Section 4. Some numerical results are presented in Section 5, while in Section 6 some concluding remarks are included.

2. Hamiltonian MG model

In this section, the model of a generic single-phase MG is presented. The model is built up by a proper interconnection of individual PCH models that represent the electrical network and the power converters, leading to a single PCH representation for the complete MG.

2.1. *Electrical network model*

The core of the MG is an electrical network that is composed by power lines that interconnect sources and loads ports. There exist three kinds of buses: grid-forming, grid-following and loads. In particular, it is assumed that there are n_1 grid-forming nodes (associated to voltage-fed converters), n_2 loads, n_3 lines and n_4 grid-following nodes (associated to current-fed converters).

In order to develop the model, it is assumed that

A.1 each power line is modelled by a series $R-L$ linear circuit,

A.2 each load and each grid-following bus has a shunt linear capacitor parallel-connected.

The dynamical variables associated with the electrical network are represented by the vector of the capacitor voltages

$$x_3 = \left[x_{3z} x_{3s}\right] \in \mathbb{R}^{(n_2+n_4)}, \tag{2.1}$$

and the vector of inductor currents $x_4 \in \mathbb{R}^{n_3}$. The voltage vector partition (2.1) is necessary to distinguish between the voltages at the grid-following buses x_{3s} and the voltages at loads' ports x_{3z}.

Considering **A.1** and **A.2**, the network composed by the interconnecting lines can be represented by an electrical circuit whose dynamics can be obtained following ideas from Graph theory (see Bollobás, 1998, and the application to MGs reported in Avila-Becerril *et al.*, 2016). To this end, assume that the electrical circuit has two kinds of input ports whose corresponding variables are given by the pair of currents and voltages $f_1,\ e_1 \in \mathbb{R}^{n_1}$ and $f_2,\ e_2 \in \mathbb{R}^{n_4}$. As will be explained below, these ports are used to interconnect the network with the voltage-fed and current-fed converters.

On the other hand, the electrical circuit total stored energy $W_{34}:\ \mathbb{R}^{(n_2+n_4)} \times \mathbb{R}^{n_3} \to \mathbb{R}_{\geqslant 0}$ is given by

$$W(x_3, x_4) = \frac{1}{2} x_3^T C x_3 + \frac{1}{2} x_4^T L x_4, \tag{2.2}$$

where $C = diag\{C_z, C_s\} = C^T > 0$ and $L = L^T > 0$ are the capacitances and inductances matrices, respectively. Concerning the dissipative elements, the constitutive relationships between the currents $i_R \in \mathbb{R}^{n_3}$ and voltages $v_R \in \mathbb{R}^{n_3}$ for the resistances in series with the line inductors, under **A.1**, are

$$i_R = x_4 = R_4^{-1} v_R, \tag{2.3}$$

with $R_4 = \text{diag}\{R_{4i}\} \in \mathbb{R}^{n_3 \times n_3}$, $R_{4i} > 0$, the resistance matrix, while the behaviour of the loads' currents $i_z \in \mathbb{R}^{n_2}$ in terms of their corresponding voltages $v_z \in \mathbb{R}^{n_2}$ is characterized by

$$i_z = \psi_c^{-1}(v_z) = \psi_c^{-1}(x_{3z}), \tag{2.4}$$

where $\psi_c(\cdot)$ is a bijective (possibly non-linear) vector function and the last identity is obtained by taking into account **A.2**. Under the conditions introduced above, the dynamical model of the network can be written as a PCH system given by

$$P_{34}\dot{x}_{34} = \left[\mathbb{J}_{34} - R_{34}\right] x_{34} - \psi_{34}(x_{3z}) + G_{34} E_s, \tag{2.5}$$

where $x_{34} = \begin{bmatrix} x_3^T & x_4^T \end{bmatrix}^T \in \mathbb{R}^{(n_2+n_4+n_3)}$, $R_{34} = \text{diag}\{R_3^{-1}, R_4\}$, $R_3 := \text{diag}\{R_{3i}\} \in^{(n_2+n_4)\times(n_2+n_4)}$ model the capacitors' losses and the matrices

$$\mathbb{J}_{34} = \begin{bmatrix} 0 & -H_{CL} \\ H_{CL}^T & 0 \end{bmatrix} = -\mathbb{J}_{34}^T, \quad G_{34} = \begin{bmatrix} 0 & -H_{C2} \\ H_{1L}^T & 0 \end{bmatrix},$$
$$P_{34} = \begin{bmatrix} C & 0 \\ 0 & L \end{bmatrix}, \quad \psi_{34}(x_{3z}) = \begin{bmatrix} H_{CZ} i_z \\ 0 \end{bmatrix}, \quad E_s = \begin{bmatrix} e_1 \\ f_2 \end{bmatrix}.$$

System (2.5) is subject to the algebraic constraints

$$f_1 = H_{1L} x_4, \tag{2.6}$$

$$e_2 = H_{C2}^T x_3, \tag{2.7}$$

where H_{CZ}, H_{1L}, H_{CL} and H_{C2} are submatrices of the *fundamental loop matrix*. The interested reader is referred to Avila-Becerril *et al.* (2016) for a detailed explanation about the structure of these matrices with respect to different network topologies. In particular, it can be proved that, as a consequence of **A.1** and **A.2**, matrices H_{CZ} and H_{C2} take the form

$$H_{CZ}^T = \begin{bmatrix} I_{n_2} & \vdots & \mathbf{0} \end{bmatrix}, \text{ and } H_{C2}^T = \begin{bmatrix} \mathbf{0} & \vdots & -I_{n_4} \end{bmatrix}. \tag{2.8}$$

2.2. *Power converters model*

For modelling the power converters, two general conditions are studied to include the phenomena generated by different kinds of DERs. It is considered that some DERs produce a voltage output signal while others provide a current output signal.

Associated with the DERs with a voltage output, there are n_1 voltage-fed converters, each one composed by a DC voltage source, a switching device and a second-order output filter. This set of converters have a stored energy function $W_1 : \mathbb{R}^{n_1} \times \mathbb{R}^{n_1} \to \mathbb{R}_{\geqslant 0}$ given by

$$W_1(x_1, x_2) = \frac{1}{2} x_1^T L_v x_1 + \frac{1}{2} x_2^T C_v x_2, \tag{2.9}$$

where $x_1 \in \mathbb{R}^{n_1}$ and $x_2 \in \mathbb{R}^{n_1}$ are the filters inductor currents and the capacitor voltages, respectively, while $L_v = L_v^T > 0$ and $C_v = C_v^T > 0$ are the $n_1 \times n_1$ inductance and capacitance matrices. With the stored energy function at hand, the dynamic behaviour of the n_1 voltage-fed converters can be represented in a compact form as

$$P_{12} \dot{x}_{12} = \left[\mathbb{J}_{12} - R_{12}\right] x_{12} + \begin{bmatrix} V u_1 \\ 0 \end{bmatrix} - \begin{bmatrix} 0 \\ I_L \end{bmatrix}, \tag{2.10}$$

with $x_{12} = \begin{bmatrix} x_1^T & x_2^T \end{bmatrix}^T \in \mathbb{R}^{2n_1}$, $R_{12} = \text{diag}\left\{0, r^{-1}\right\}$, $r^{-1} = \text{diag}\{r_i^{-1}\}$, $i = 1, \ldots, n_1$ the filters capacitor losses, $P_{12} = diag\{L_v, C_v\}$ and

$$\mathbb{J}_{12} = \begin{bmatrix} 0 & -I \\ I & 0 \end{bmatrix} = -\mathbb{J}_{12}^T \in \mathbb{R}^{2n_1 \times 2n_1}.$$

In this representation, the vector $u_1 = col\{u_{1i}\} \in \mathbb{R}^{n_1}$ is composed by the control input of each converter and $V = \text{diag}\{V_i\} \in \mathbb{R}^{n_1 \times n_1}$ is the matrix of constant voltage sources $V_i > 0$.

For the set of DERs with current output, there exist n_4 current-fed power converters whose individual structure is given by a capacitor parallel connected to a DC current source, a switching device and an output inductor. For this set of devices, the stored energy function $W_2 : \mathbb{R}^{n_4} \times \mathbb{R}^{n_4} \to \mathbb{R}_{\geqslant 0}$ takes the form

$$W_2(x_5, x_6) = \frac{1}{2} x_5^T L_f x_5 + \frac{1}{2} x_6^T C_f x_6, \tag{2.11}$$

with $x_5 \in \mathbb{R}^{n_4}$ and $x_6 \in \mathbb{R}^{n_4}$ the inductor currents and the capacitor voltages, respectively, and $L_f = L_f^T > 0$, $C_f = C_f^T > 0$ the $n_4 \times n_4$ inductance and capacitance matrices. Hence, defining $P_{56} = \text{diag}\{L_f, C_f\}$, the dynamic behaviour of the n_4 current-fed converters can be represented by

$$P_{56}\dot{x}_{56} = \left[\mathbb{J}_{56}(U_2) - R_{56}\right] x_{56} + \epsilon, \tag{2.12}$$

where $x_{56} = \begin{bmatrix} x_5^T & x_6^T \end{bmatrix}^T \in \mathbb{R}^{2n_4}$, $R_{56} = \text{diag}\{R_f, r_f^{-1}\}$, the inductor and capacitor losses given by $R_f = \text{diag}\{R_{fi}\}$ and $r_f^{-1} = \text{diag}\{r_{fi}^{-1}\}$, $i = 1, \ldots, n_4$ and the matrices

$$\mathbb{J}_{56}(U_2) = \begin{bmatrix} 0 & U_2 \\ -U_2 & 0 \end{bmatrix} = -\mathbb{J}_{56}^T(U_2) \in \mathbb{R}^{2n_4 \times 2n_4}, \quad \epsilon = \begin{bmatrix} -E \\ I_0 \end{bmatrix},$$

with $U_2 = \text{diag}\{u_{21}, \ldots, u_{2n4}\}$ and $I_0 = col\{I_{0i}\} \in \mathbb{R}^{n_4}$ the vector of constant current sources $I_{0i} > 0$. The vector $E = col\{E_i\} \in \mathbb{R}^{n_4}$ is composed by the port voltages of the network where the current-fed converters are connected.

At this point, it is useful to recover the result reported in Cisneros *et al.* (2015) which states that under an appropriate definition of constant skew-symmetric matrices J_i, $i = 1, \ldots, n_4$, the matrix $\mathbb{J}_{56}(U_2)$ can be written as

$$\mathbb{J}_{56}(U_2) = J_1 u_{21} + \ldots + J_{n4} u_{2n4}, \tag{2.13}$$

leading to the possibility of obtaining the alternative representation of model (2.12) given by

$$P_{56}\dot{x}_{56} = -R_{56} x_{56} + G_2(x_{56}) u_2 + \epsilon, \tag{2.14}$$

where $u_2 = col\left\{u_{2i}\right\}$ and

$$G_2(x_{56}) := \left[J_1 x_{56} \ \vdots \ \ldots \ \vdots \ J_{n4} x_{56} \right]. \tag{2.15}$$

As will be clear below, the property above is fundamental in the development of the control scheme considered in this paper since the vector control input u_2 appears in an affine way in the alternative model (2.14).

2.3. *Complete MG model*

The complete dynamical model of the MG can be obtained by interconnecting the input ports of the electrical circuit with the output ports of the voltage-fed and current-fed converters. This is done by identifying that the constraints given by

$$f_1 = I_L = H_{1L}x_4, \tag{2.16a}$$

$$e_1 = x_2, \tag{2.16b}$$

$$e_2 = E = H_{C2}^T x_3, \tag{2.16c}$$

$$f_2 = -x_5 \tag{2.16d}$$

must be satisfied. Moreover, since these equations naturally define power preserving interconnections, (van der Schaft & Maschke, 2013), then it is possible to conclude that the resulting complete system also exhibits a PCH structure.

The complete MG model considers the vector state

$$x = \begin{bmatrix} x_1^T & x_2^T & x_3^T & x_4^T & x_5^T & x_6^T \end{bmatrix}^T \in \mathbb{R}^n$$

with dimension $n = 2n_1 + n_2 + n_3 + 3n_4$. Thus, the total stored energy function of the whole system is

$$W_T(x) = x^T P x, \tag{2.17}$$

with $P = \text{diag}\{P_{12}, P_{34}, P_{56}\} = P^T > 0$, leading to the complete model given by

$$P\dot{x} = \left[\mathbb{J}_T(U_2) - \mathbb{R}_T\right]x + \mathbb{V}u_1 + \mathbb{I}_0 - \Psi_{34}(x_{3_z}), \tag{2.18}$$

with $\mathbb{R}_T = \text{diag}\{0, r^{-1}, R_3^{-1}, R_4, R_f, r_f^{-1}\} = \mathbb{R}_T^\top \geqslant 0$ and the matrices

$$\mathbb{J}_T = \begin{bmatrix} 0 & -I & 0 & 0 & 0 & 0 \\ I & 0 & 0 & -H_{1L} & 0 & 0 \\ 0 & 0 & 0 & -H_{CL} & H_{C2} & 0 \\ 0 & H_{1L}^T & H_{CL}^T & 0 & 0 & 0 \\ 0 & 0 & -H_{C2}^T & 0 & 0 & U_2 \\ 0 & 0 & 0 & 0 & -U_2 & 0 \end{bmatrix}, \mathbb{V} = \begin{bmatrix} V \\ 0 \\ 0 \\ 0 \\ 0 \\ 0 \end{bmatrix},$$

$$\mathbb{I}_0 = \begin{bmatrix} 0 \\ 0 \\ 0 \\ 0 \\ 0 \\ I_0 \end{bmatrix}, \ \Psi_{34}(x_{3_z}) = \begin{bmatrix} 0 \\ 0 \\ H_{CZ}\psi_c^{-1}(x_{3_z}) \\ 0 \\ 0 \\ 0 \end{bmatrix}.$$

If property (2.14) is considered, model (2.18) can be equivalently written as the input-affine non-linear system

$$P\dot{x} = \left[\mathbb{J}_0 - \mathbb{R}_T\right] x + \mathbb{G}_T(x_{56})u + \mathbb{I}_0 - \Psi_{34}(x_{3z}), \tag{2.19}$$

where $u = \left[u_1^T \;\; u_2^T\right]^T \in \mathbb{R}^{n_1+n_4}$, $\mathbb{V}_1 = col\{V, 0, 0, 0\}$ and

$$\mathbb{G}_T(x_{56}) := \begin{bmatrix} \mathbb{V}_1 & \vdots & \mathbf{0} \\ \mathbf{0} & \vdots & G_2(x_{56}) \end{bmatrix}, \tag{2.20}$$

with $G_2(x_{56})$ already defined in (2.15).

REMARK 2.1 It is interesting to point out that although the use of the developed model will be specialized to the case of alternate current (AC) networks, it *verbatim* applies for the study of DC operation. This degree of freedom can be used to extend the results presented in this paper. Current research is carried out in this sense.

3. Passivity-based control design

In this section, the design of the proposed control law for the MG model (2.19) is introduced. However, before presenting this scheme, it is important to recognize a useful structural property of the system that is evidenced by the decomposition into subsystems introduced in Section 2. This property refers to the fact that the fulfillment of a power demanded by the loads is guaranteed if the converters' voltages and currents, x_{12} and x_{56}, reach appropriate (prescribed) values, leaving the variables related to the power lines, x_{34}, with the possibility of evolving in a free way (as long as they remain bounded). The last is possible since, if the sources can provide a demanded amount of power, the power balance is achieved with the variables x_{34} naturally tending to some (bounded) value that corresponds to this operating condition. Hence, only for systems (2.10) and (2.12), it is necessary to include a control scheme, while system (2.5) can freely evolve.

On the other hand, a second feature of the control problem that must be taken into account concerns with the condition that, from a technical perspective, the control schemes for systems (2.10) and (2.12) deal with a tracking control problem for the output variables of the power converters. Thus, before developing the control law, a previous step that is necessary to cover is the identification of the constraints that the reference operating conditions must satisfy. These constraints are imposed by the system's model so that the admissible reference trajectories must be solution of

$$P_{12}\dot{x}_{12}^\star = (\mathbb{J}_{12} - R_{12})x_{12}^\star + \begin{bmatrix} Vu_1^\star \\ 0 \end{bmatrix} - \begin{bmatrix} 0 \\ H_{1L}x_4 \end{bmatrix}, \tag{3.1a}$$

$$P_{56}\dot{x}_{56}^\star = -R_{56}x_{56}^\star + G_2^\star(x_{56}^\star)u_2^\star + \begin{bmatrix} -H_{C2}^T x_3 \\ I_0 \end{bmatrix}, \tag{3.1b}$$

where the line variables x_{34} are considered as externally known signals and $u_1^\star$, $u_2^\star$ are the control inputs that generate the references $x_{12}^\star$ and $x_{56}^\star$, respectively.

With the preliminaries stated above, to formulate the control problem for the power converters, it is convenient to define the error variables $\tilde{x}_i = x_i - x_i^\star$, $i = 12, 56$, and the corresponding error dynamic given by

$$P_{12}\dot{\tilde{x}}_{12} = \left[\mathbb{J}_{12} - R_{12}\right]\tilde{x}_{12} + \begin{bmatrix} V\tilde{u}_1 \\ 0 \end{bmatrix}, \tag{3.2a}$$

$$P_{56}\dot{\tilde{x}}_{56} = \left[\mathbb{J}_{56}(U_2) - R_{56}\right]\tilde{x}_{56} + G_2(x_{56}^\star)\tilde{u}_2, \tag{3.2b}$$

where the last equation is obtained by exploiting the alternative representation (2.14). Under these conditions, the control problem is formulated as to design control inputs u_1 and u_2 such that

$$\lim_{t\to\infty} \tilde{x}_{12} = 0; \quad \lim_{t\to\infty} \tilde{x}_{56} = 0.$$

The solution proposed in this paper to this problem is presented in the next proposition.

PROPOSITION 3.1 Consider the MG model (2.19). Assume **A.1** and **A.2** are satisfied. Additionally, consider that

- **A.3** currents x_1, x_5 and voltages x_6 are available for measurement,
- **A.4** the converters parameters P_{12} and P_{56} are known,
- **A.5** the prescribed voltage $x_2^\star$ and current $x_5^\star$ are known bounded continuous functions with a bounded second derivative,
- **A.6** the load port variables satisfy the passivity condition

$$x_{3z}^T \psi_c^{-1}(x_{3z}) \geqslant 0.$$

Under these conditions, the control laws given by

$$u_1 = -V^{-1}K_{p1}\tilde{x}_1 + u_1^\star; \quad K_{p1} = K_{p1}^T > 0 \tag{3.3a}$$

$$u_2 = -K_{p2}y_2 + u_2^\star; \quad K_{p2} = K_{p2}^T > 0 \tag{3.3b}$$

with $y_2 := G_2^T(x_{56}^\star)\tilde{x}_{56}$, and $u_1^\star$, $u_2^\star$ satisfying (3.1), achieve

$$\lim_{t\to\infty} \tilde{x}_{12} = 0; \quad \lim_{t\to\infty} \tilde{x}_{56} = 0$$

guaranteeing internal stability.

Proof. The proof is based on cascade arguments; see Sepulchre *et al.* (2012). First, notice that the system (3.2) in closed-loop with control (3.3) can be written as

$$\begin{bmatrix} P_{12}\dot{\tilde{x}}_{12} \\ P_{56}\dot{\tilde{x}}_{56} \end{bmatrix} = \begin{bmatrix} \mathbb{J}_{12} - \bar{R}_{12} & 0 \\ 0 & \mathbb{J}_{56}(U_2) - R_{56} \end{bmatrix} \begin{bmatrix} \tilde{x}_{12} \\ \tilde{x}_{56} \end{bmatrix} - \begin{bmatrix} 0 \\ G_2(x_{56}^\star)K_{p2}y_2 \end{bmatrix}, \tag{3.4}$$

where $\bar{R}_{12} = \text{diag}\{K_{p1}, r^{-1}\} = \bar{R}_{12}^T > 0$. By defining the auxiliary variable $\zeta = \begin{bmatrix}\tilde{x}_{12}^T & \tilde{x}_{56}^T\end{bmatrix}^T$, the closed-loop system (3.4) takes the form

$$\bar{P}\dot{\zeta} = \left[\bar{J}(U_2) - \bar{R}\right]\zeta - \begin{bmatrix} 0 \\ G_2(x_{56}^\star)K_{p2}y_2 \end{bmatrix}, \tag{3.5}$$

with $\bar{P} = \text{diag}\{P_{12}, P_{56}\} = \bar{P}^\top > 0$, $\bar{R} = \text{diag}\{\bar{R}_{12}, R_{56}\} = \bar{R}^T > 0$ and $\bar{J}(U_2) = \text{diag}\{\mathbb{J}_{12}, \mathbb{J}_{56}(U_2)\} = -\bar{J}^T(U_2)$.

On the other hand, under the port interconnections (2.16b) and (2.16d), the network dynamic (2.5) is given by

$$P_{34}\dot{x}_{34} = \left[\mathbb{J}_{34} - R_{34}\right]x_{34} - \psi_{34}(x_{3z}) + A\begin{bmatrix}\tilde{x}_{12} + x_{12}^\star \\ \tilde{x}_{56} + x_{56}^\star\end{bmatrix}, \tag{3.6}$$

with

$$A := \begin{bmatrix} 0 & 0 & H_{C2} & 0 \\ 0 & H_{1L}^T & 0 & 0 \end{bmatrix}.$$

Thus, by defining $= \begin{bmatrix}x_{12}^{\star T} & x_{56}^{\star T}\end{bmatrix}$, the whole system exhibits the cascade structure

$$\dot{\zeta} = g(\zeta, \zeta^\star), \tag{3.7a}$$

$$\dot{x}_{34} = f(x_{34}) + \Gamma(\zeta, \zeta^\star), \tag{3.7b}$$

where $\Gamma(\zeta, \zeta^\star) = A(\zeta + \zeta^\star)$ while $g(\zeta, \zeta^\star)$ and $f(x_{34})$ can be directly identified from (3.4) and (3.6), respectively.

In the rest of the proof, it is shown that $\Gamma(\zeta, \zeta^\star)$ is a non-vanishing but bounded perturbation when $\zeta = 0$, that subsystem (3.7a) is globally exponentially stable (GES) and that the subsystem (3.7b) is input-to-state stable (ISS), permitting the application of well-known results of cascaded systems theory to obtain the stated stability properties.

Concerning the analysis of (3.7a), consider the Lyapunov function

$$V_1(\zeta) = \frac{1}{2}\zeta^T\bar{P}\zeta, \tag{3.8}$$

with $\bar{P} = \bar{P}^T > 0$, such that

$$\lambda_{\min}(\bar{P})|\zeta|^2 \leqslant V_1(\zeta) \leqslant \lambda_{\max}(\bar{P})|\zeta|^2.$$

Taking its time derivative of (3.8) along the trajectories of (3.7a) yields

$$\begin{aligned}\dot{V}_1(\zeta) =& -\zeta^T\bar{R}\zeta - y_2^T K_{p2} y_2 \\ &\leqslant -\zeta^T\bar{R}\zeta \leqslant -\lambda_{\min}(\bar{R})|\zeta|^2,\end{aligned}$$

proving the GES property of the equilibrium $\zeta = 0$.

In order to formulate the ISS properties of subsystem (3.7b), consider first its dynamic behaviour when $\Gamma(\zeta, \zeta^\star) = 0$, given by

$$\dot{x}_{34} = f(x_{34}). \tag{3.9}$$

Under this condition, take the positive definite function

$$W(x_{34}) = \frac{1}{2} x_{34}^T P_{34} x_{34}, \tag{3.10}$$

whose time derivative along the trajectories of (3.9) is

$$\begin{aligned}\dot{W}(x_{34}) = \left(\frac{\partial W(x_{34})}{\partial x_{34}}\right)^T f(x_{34}) &= x_{34}^T \left(\left[\mathbb{J}_{34} - R_{34}\right] x_{34} - \psi_{34}(x_{3_z})\right) \\ &= -x_{34}^T R_{34} x_{34} - x_3^T H_{CZ} \psi_c^{-1}(x_{3_z}).\end{aligned}$$

Taking into account Assumption **A.6** and the definition of H_{CZ} in (2.8), gives as a result, invoking La Salle invariance principle, that the equilibrium $x_{34} = 0$ is GAS.

On the other hand, consider the presence of the perturbation term $\Gamma(0, \zeta^\star)$, i.e., when $\zeta = 0$, which due to **A.5** is bounded. Under this condition, the time derivative of (3.10) along (3.7b) takes the form

$$\begin{aligned}\dot{W}(x_{34}) &= -x_{34}^T R_{34} x_{34} - x_3^T H_{CZ} \psi_c^{-1}(x_{3_z}) + x_{34}^\top \Gamma(0, \zeta^\star) \\ &\leqslant -(1-\theta)\lambda_{\min}(R_{34})|x_{34}|^2 - \theta\lambda_{\min}(R_{34})|x_{34}|^2 + |x_{34}||\Gamma(0, \zeta^\star)|,\end{aligned}$$

with $0 < \theta < 1$. Thus,

$$\dot{W}(x_{34}) \leqslant -(1-\theta)\lambda_{\min}(R_{34})|x_{34}|^2,$$

provided

$$|x_{34}| \geqslant \frac{|\Gamma(0, \zeta^\star)|}{\theta\lambda_{\min}(R_{34})}.$$

Hence, it is concluded that the system (3.7b) is ISS, so that

$$|x_{34}(t)| \leqslant \beta(|x_{34}(t_0)|, t - t_0) + \gamma\left(\sup_{\tau \geqslant t_0} |\Gamma(0, \zeta^\star)|\right), \quad \forall t \geqslant t_0,$$

with β a *KL* function and $\gamma(r) = \sqrt{\frac{\lambda_{\max}(P_{34})}{\lambda_{\min}(P_{34})}} \frac{r}{\theta\lambda_{\min}(R_{34})}$.

The proof is finished exploiting argument of cascaded systems theory (for example, Sepulchre *et al.*, 2012, Proposition 4.1) noticing that the GES system (3.7a) is interconnected with the ISS system (3.7b) via a term that satisfies $|\Gamma(\zeta, \zeta^\star)| \leqslant |A||\zeta| + \gamma_2$ for a positive constant γ_2 and leading to the conclusion that the equilibrium point $(x_{34}, \zeta) = (x_{34}^\star, 0)$ is GAS.

□

The following remarks about the presented result are in order.

REMARK 3.1 It is important to point out that the bounded behaviour of the whole closed-loop system is guaranteed as long as the variables $x_2^\star$ and $x_5^\star$ are also bounded. Moreover, as the output voltage of the voltage-fed converters tends to the former, while the output current of the current-fed converters tends to the latter, then the generation of grid-forming and grid-following nodes, respectively, is assured by a proper selection of $x_2^\star$ and $x_5^\star$.

REMARK 3.2 It is also interesting to note that the selection of $x_2^\star$ and $x_5^\star$ imposes the network operation condition. In the next section, the particular case of AC networks is approached. However, there exists the possibility of considering the DC operation case under a proper definition of the reference variables. Current research is carried out considering this context.

4. Reference variable design

The last step in the controller design involves two computations, namely the determination of the reference variables $x_{12}^\star$, $x_{56}^\star$ for given $x_2^\star$, $x_5^\star$, and the explicit selection of these last variables to achieve voltage regulation and power network balance.

In order to perform the first computations, notice that, from (3.1a), an admissible behaviour $x_{12}^\star$ must satisfy the equations

$$L_v\dot{x}_1^\star = -x_2^\star + Vu_1^\star, \tag{4.1a}$$

$$C_v\dot{x}_2^\star = x_1^\star - H_{1L}x_4. \tag{4.1b}$$

Therefore, if an output voltage $x_2^\star$ for the voltage-fed converters is imposed, the required input to generate it is

$$u_1^\star = V^{-1}\left[L_v\dot{x}_1^\star + x_2^\star\right], \tag{4.2}$$

with the corresponding value for $x_1^\star$ is obtained as

$$x_1^\star = -C_v\dot{x}_2^\star - H_{1L}x_4.$$

Regarding the structure of the last expression, it is worth pointing out its fundamental role in the solution proposed in this paper. Notice that the admissible value of the current $x_1^\star$ is naturally adjusted in terms of the network operation conditions expressed by the total current $H_{1L}x_4$. In particular, any change in power demanded by the loads is translated into a variation of x_4 and, consequently, into an adaptation of the reference value $x_1^\star$. This feature is exploited below to solve the power balance objective.

On the other hand, from (3.1b), any admissible behaviour $x_{56}^\star$ must be solution of

$$L_f\dot{x}_5^\star = -R_fx_5^\star + \mathrm{diag}\{x_{6i}^\star\}u_2^\star - H_{C2}^Tx_3, \tag{4.3a}$$

$$C_f\dot{x}_6^\star = -r_f^{-1}x_6^\star - \mathrm{diag}\{x_{5i}^\star\}u_2^\star + I_0. \tag{4.3b}$$

Thus, for a prescribed output current $x_5^\star$ for the current-fed converters, the corresponding value for $x_6^\star$ is obtained as solution of (4.3b) while the required input for generating $x_{56}^\star$ takes the form

$$u_2^\star = \left[G_2^\top(x_{56}^\star)G_2(x_{56}^\star)\right]^{-1} G_2^\top(x_{56}^\star)\left(P_{56}\dot{x}_{56}^\star + R_{56}x_{56}^\star + \begin{bmatrix} H_{C2}^T x_3 \\ -I_0 \end{bmatrix}\right). \tag{4.4}$$

The implementation of (4.4) is possible due to the fact that $G_2(x_{56}^\star)$ is column full rank for all $x_{56}^\star \neq 0$.

Once the procedure to determine the values of $x_{12}^\star$ and $x_{56}^\star$ has been established, the second computation, required to complete the last step of the controller design, concerns to the explicit definition of $x_2^\star$ and $x_5^\star$. In this sense, the former is devoted to guarantee the generation of grid-forming nodes while the latter is dedicated to achieve a prescribed power generation, relating the operation of the current-fed converters with grid-following nodes.

Concerning the voltage regulation objective, it is immediate to recognize that the output voltage of the i-th voltage-fed converter must exhibit the form

$$x_{2i}^\star = \sqrt{2}V_i^{rms}\cos(\omega t + \theta_{Vi}), \tag{4.5}$$

where V_i^{rms} is the root-mean square (RMS) desired voltage magnitude while ω and θ_{Vi} are its angular frequency and phase, respectively. At this point, it must be noticed that if the angular frequency ω is the same for all the grid-forming nodes, then synchronization of the network is achieved. Furthermore, although the phase angle θ_{Vi} can be viewed as an additional degree of freedom, for generation of voltage reference nodes, the usual assigned value is zero.

Regarding the power balance objective, the premise to state the proposed solution is that the power demanded by the loads must be satisfied in conjunction with the grid-following and the grid-forming nodes. To do this, it is considered that the sources associated with grid-following nodes have a limited power generation capacity. Thus, the objective is to force these nodes to provide their maximum available power and complement the demand with power provided by the grid-forming nodes. In this sense, it is assumed that the voltage-fed converters can always deliver the current $x_1^\star$ imposed by a specific value of x_4 leading to the fact that, without explicitly knowing the power demanded by the loads, the desired power network balance is achieved since the grid-forming nodes are always capable of contributing with the required power.

Under the scenario described above, consider that the i-th grid-following converter can deliver only a fixed amount of active and reactive powers denoted by $P_{gi}^\star$ and $Q_{gi}^\star$, respectively. In addition, assume that the point of common coupling between this converter and the grid has a well-defined voltage profile, provided by the grid-forming nodes, of the form

$$E_i = \sqrt{2}E_i^{rms}\cos(\omega t + \theta_{Ei}). \tag{4.6}$$

This condition, in its turn, implies that the admissible output current $x_{5i}^\star$ of the current-fed converters must be exhibit also a sinusoidal structure which, using well-known arguments from AC circuits, can be written as

$$x_{5i}^\star = \frac{1}{\sqrt{2}E_i^{rms}}\left[P_{gi}^\star\cos(\omega t + \theta_{Ei}) + Q_{gi}^\star\sin(\omega t + \theta_{Ei})\right], \tag{4.7}$$

TABLE 1 *Test system parameters*

Parameter	Value	Parameter	Value	Parameter	Value
C_i	150 μF	C_j	200 μF	C_k	200 μF
C_k	60 μF	R_{si}	60 mΩ	L_{si}	1.25 mH
R_{ij}	10 mΩ	L_{ij}	1.25 mH	R_{jk}	50 mΩ
L_{jk}	1.25 mH	R_{jl}	10 mΩ	L_{jl}	100 μH
R_{km}	10 mΩ	L_{km}	2.5 mH	R_{ln}	1 mΩ
L_{ln}	2.5 mH	R_j	6Ω	$R_j = R_k$	5 Ω
f	60 Hz	V_{rms}	$\frac{220}{\sqrt{3}}$ V	V_{DC}	600 V

where the relationship between the parallel and quadrature components of the voltage profile and the active and reactive powers has been used.

Implementation of (4.7) can be carried out noting that the parallel component of the voltage profile is given by

$$e_{\parallel} = \frac{1}{\sqrt{2}E_i^{rms}} E_i = \cos(\omega t + \theta_{Ei}). \tag{4.8}$$

Hence, the quadrature component $e_{\perp}$ can be reconstructed by the use of a classical quadrature generator of the form

$$\begin{bmatrix} \dot{z}_1 \\ \dot{z}_2 \end{bmatrix} = \begin{pmatrix} -k_s & \omega \\ -\omega & 0 \end{pmatrix} \begin{bmatrix} z_1 \\ z_2 \end{bmatrix} + \begin{bmatrix} k_s \\ 0 \end{bmatrix} e_{\parallel} \tag{4.9}$$

due to the fact that, if $k_s > 0$, the solutions z_1 and z_2 of this dynamical system asymptotically converge to $e_{\parallel}$ and $e_{\perp}$, respectively, with a rate of convergence determined by k_s. Thus, the implementable version of (4.7) is given by

$$x_{5i}^{\star} = \frac{1}{\sqrt{2}E_i{}^{rms}} \left(P_{gi}^{\star} z_1 + Q_{gi}^{\star} z_2 \right). \tag{4.10}$$

5. Test system and simulation results

In this section, the usefulness of the proposed controller is evaluated via a numerical simulation. The considered MG, shown in Fig. 1, is composed by one voltage-fed converter, two current-fed converters, three transmission lines and five loads. From the perspective of model (2.18), the corresponding matrices are given by

$$H_{1L}^{\top} = \begin{bmatrix} 1 \\ 0 \\ 0 \end{bmatrix}, \quad H_{CL} = \begin{bmatrix} -1 & -1 & -1 \\ 0 & 1 & 0 \\ 0 & 0 & 1 \end{bmatrix}, \quad H_{C2} = \begin{bmatrix} 0 & 0 \\ -1 & 0 \\ 0 & -1 \end{bmatrix} \quad \text{and} \quad H_{CZ} = \begin{bmatrix} 1 & 0 & 0 \\ 0 & 1 & 0 \\ 0 & 0 & 1 \end{bmatrix}, \tag{5.1}$$

while $n_1 = 1$ and $n_4 = 2$. The considered parameters for the network are listed in Table 1.

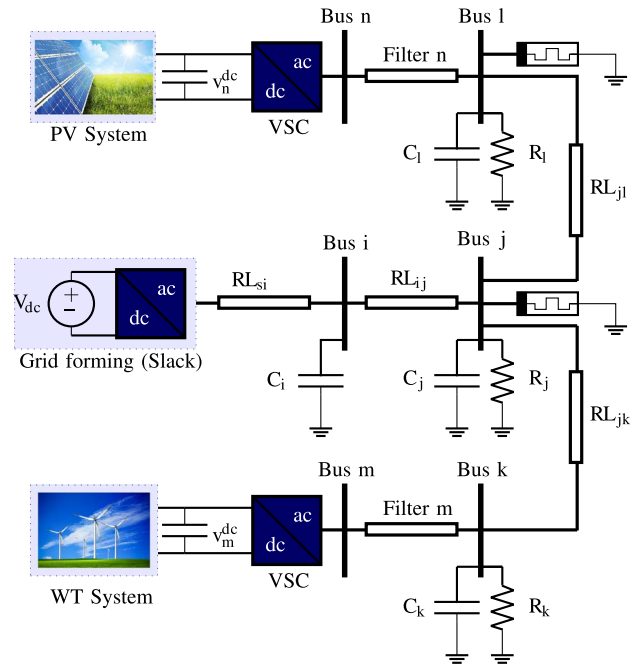

FIG. 1. Electrical configuration of a single-phase MG for isolating grid applications.

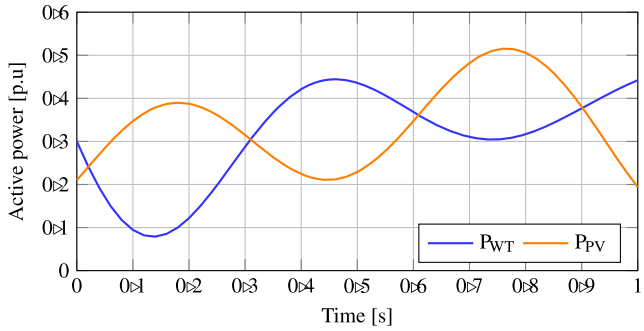

FIG. 2. Active power available in the renewable energy resources.

With the aim to carry the evaluation out as close as possible to a realistic scenario, several practical features were introduced, namely

- instead of consider the averaged model, the simulation was implemented in the SimPowerSystems library of MATLAB/Simulink using switching models for the converters, operating at a 10 kHz switching frequency;
- a battery energy storage replaced the voltage source of the voltage-fed converter;

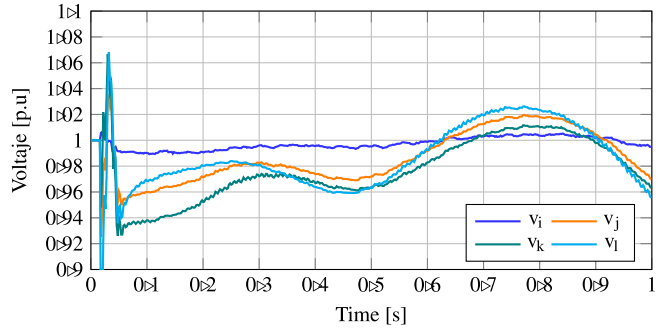

FIG. 3. Voltage RMS values in all nodes of the network.

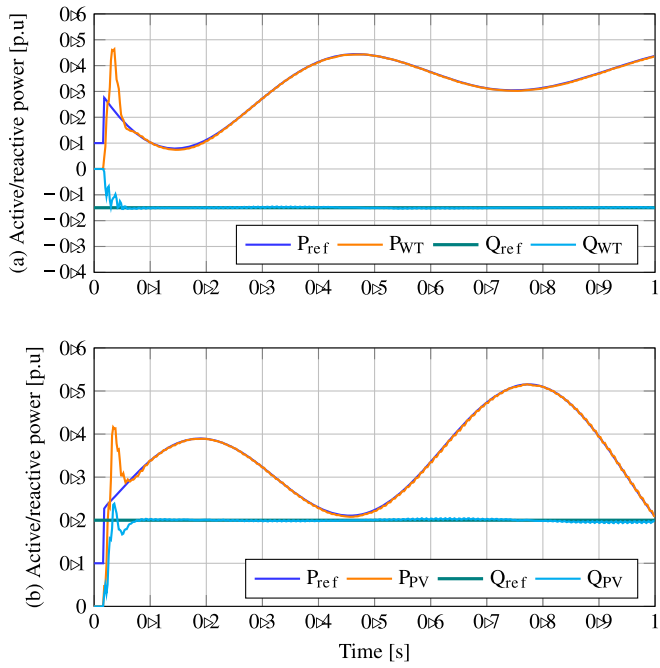

FIG. 4. Active and reactive power outputs in the renewable energy resources: (a) WT generation system and (b) PV system.

- the current sources of the two current-fed converters were implemented using a 600-V base PV unit and a 10-kW power base wind turbine (WT). Concerning their power capacity, Fig. 2 shows the time-varying power available at the PV and WT generation systems.
- In addition to passive loads, given in this case by *RC* arrays, constant power loads (CPLs) were parallel connected at the j and l buses considering that they consume, under nominal voltage operative conditions, 8 kW, 5 kVAr and 6 kW, 4 kVAr, respectively.

Under the conditions described above, the purpose of the simulation was to validate that for the power demand imposed by the mixed loads, the grid-forming node was able to guarantee voltage

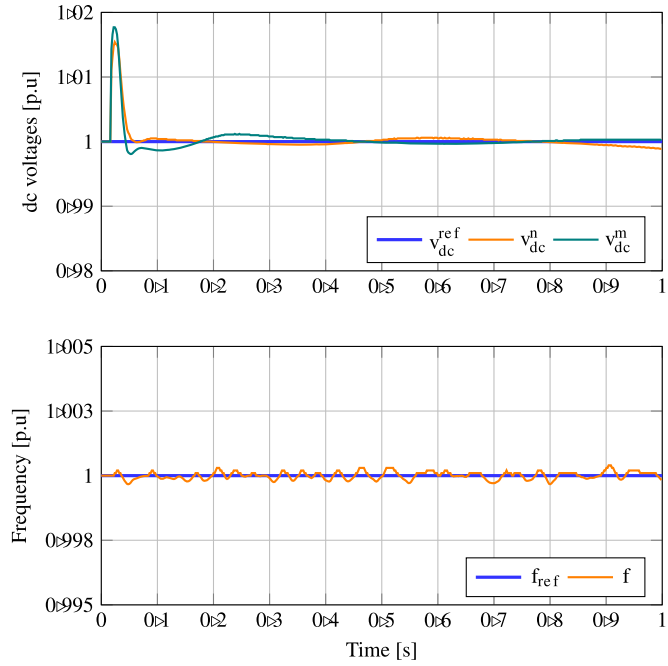

FIG. 5. Voltage performances at the DC links and grid frequency behaviour: (a) DC voltage output and (b) AC frequency performance.

regulation and the grid-following nodes assured the injection of the maximum amount of power available at their corresponding sources.

5.1. *Simulation results*

Figure 3 presents the RMS values of the voltage profiles in all the nodes of the network, where it can be noticed that they oscillate between 0.9 p.u. and 1.1 p.u., achieving voltage regulation from a practical perspective and also illustrating the stability properties of the control system. Moreover, this behaviour holds the constraint imposed by regulatory entities that allow a voltage regulation limit of ± 10 % for low-voltage distribution systems.

Figure 4 shows the active and reactive power performance of the PV and WT generation systems. As predicted by the theory and after a short transient behaviour, these systems are controlled so that all active power available on the DC side of the converters is transferred to the AC side. In addition, it is also evidenced that power converters can be effectively used to provide reactive power support to the AC grid. In particular, for the case of the WT system a constant demand of 1.5kVAr is satisfied as can be seen in Fig. 4(a), while the PV unit provides to the AC grid 2kVAr as shown in Fig. 4(b).

It is important to mention that the transient behaviour exhibited during 0.0 s to 0.1 s corresponds to the simulation's initialization and does not compromise the system's stability. Another important feature appears when active and reactive power references are reached since the maximum tracking errors are less than 2%, which confirms the possibility of operating the network in islanded mode with minimal errors despite the presence of unknown CPLs.

Finally, Fig. 5 depicts the voltage profiles at the DC sides of the converters as well as the frequency behaviour of the AC side, showing that the synchronization objective is also achieved, guaranteeing internal stability. The performance is also prominent from the application viewpoint since both voltage profiles fluctuate about their nominal values with tracking errors less than 1.775% and 1.536% for the PV and WT systems, respectively. Notice that the higher values occur during the transient state from 0.0 s to 0.1 s. On the other hand, Fig. 5(b) shows the frequency behaviour of the AC grid, which is measured at the *i*-node. This frequency oscillates around its nominal value with peaks less than $3.75 \times 10^{-2}\%$, which clearly confirms that the grid-forming node allows controlling the AC voltage profile of the whole MG.

6. Conclusions

In this paper, a solution to the voltage regulation and power balance problems for MGs operating in islanded mode was presented. The considered model for the network explicitly includes models of both the power converters associated with the DERs and the network itself, and the stability properties of the whole closed-loop system were formally proved. The main feature of the controller design methodology is given by the decomposition of the system into two kinds of subsystems, those that require a control scheme and other whose variables can evolve in a free way. Under this perspective, the power balance objective is achieved without explicit knowledge of the power demanded by the loads. From the technical viewpoint, the proposed control laws were obtained using PBC arguments, guaranteeing the generation of grid-forming and grid-following nodes, while the stability analysis was carried out complementing the PBC design with cascaded systems theory arguments. The usefulness of the contribution was validated via a simulation that considered several practical conditions.

Funding

Universidad Nacional Autónoma de México–Programa de Apoyo a Proyectos de Investigación e Innovación Tecnológica (UNAM-PAPIIT IA103519 to S.A.-B, UNAM-PAPIIT IN118019 to G.E.-P.). Colombian Ministry of Science (project 111077657914, contract number 031-2018 to A.G.)

References

Arani, A. K., Karami, H., Gharehpetian, G. B. & Hejazi, M. S. A. (2017) Review of flywheel energy storage systems structures and applications in power systems and microgrids. *Renew. Sust. Energ. Rev.*, **69**, 9–18.

Agundis-Tinajero, G., Segundo-Ramirez, J., Visairo-Cruz, N., Savaghebi, M., Guerrero, J. M. & Barocio, E. (2019) Power flow modeling of islanded AC microgrids with hierarchical control. *Int. J. Electr. Power Energy Syst.*, **105**, 28–36.

Avila-Becerril, S. & Espinosa-Pérez, G. (2020) Control of islanded microgrids considering power converter dynamics. *Int. J. Control.*, 1–11. https://doi.org/10.1080/00207179.2020.1713402.

Avila-Becerril, S., Espinosa-Pérez, G. & Machado, J. E. (2019) On the dynamic solution of power flow equations for microgrids control. *2019 58th IEEE Conference on Decision and Control (CDC)*. Nice, France, pp. 8423–8428.

Avila-Becerril, S., Montoya, O. D., Espinosa-Pérez, G. & Garcés, A. (2018) Control of a detailed model of microgrids from a Hamiltonian approach. *IFAC-PapersOnLine*, **51**, 187–192.

Avila-Becerril, S., Espinosa-Pérez, G. & Fernandez, P. (2016) Dynamic characterization of typical electrical circuits via structural properties. *Math. Probl. Eng.*, **2016**. https://doi.org/10.1155/2016/7870462.

Bidram, A., Nasirian, V., Davoudi, A. & Lewis, F. L. (2017) *Cooperative Synchronization in Distributed Microgrid Control*. Springer International Publishing.

Bollobás, B. (1998) *Modern Graph Theory*, vol. 184. Springer Science & Business Media.

Bouzid, A. M., Guerrero, J. M., Cheriti, A., Bouhamida, M., Sicard, P. & Benghanem, M. (2015) A survey on control of electric power distributed generation systems for microgrid applications. *Renew. Sust. Energ. Rev.*, **44**, 751–766.

Cisneros, R., Pirro, M., Bergna, G., Ortega, R., Ippoliti, G. & Molinas, M. (2015) Global tracking passivity-based PI control of bilinear systems: application to the interleaved boost and modular multilevel converters. *Control. Eng. Pract.*, **43**, 109–119.

Gu, W., Wu, Z., Bo, R., Liu, W., Zhou, G., Chen, W. & Wu, Z. (2014) Modeling, planning and optimal energy management of combined cooling, heating and power microgrid: a review. *Int. J. Electr. Power Energy Syst.*, **54**, 26–37.

Han, H., Hou, X., Yang, J., Wu, J., Su, M. & Guerrero, J. M. (2015) Review of power sharing control strategies for islanding operation of AC microgrids. *IEEE Trans. Smart Grid*, **7**, 200–215.

Jayachandran, M. & Ravi, G. (2019) Decentralized model predictive hierarchical control strategy for islanded AC microgrids. *Electr. Power Syst. Res.*, **170**, 92–100.

Konstantopoulos, G., Zhong, Q. C., Ren, B. & Krstic, M. (2015) Bounded droop controller for parallel operation of inverters. *Automatica*, **53**, 320–328.

Pogaku, N., Prodanovic, M. & Green, T. C. (2007) Modeling, analysis and testing of autonomous operation of an inverter-based microgrid. *IEEE Trans. Power Electron.*, **22**, 613–625.

Rojas, A. & Rousan, T. (2017) Microgrid control strategy: derived from stakeholder requirements analysis. *IEEE Power Energy Mag.*, **15**, 72–79.

Schiffer, J., Ortega, R., Astolfi, A., Raisch, J. & Sezi, T. (2014) Conditions for stability of droop-controlled inverter-based microgrids. *Automatica*, **50**, 2457–2469.

Sepulchre, R., Jankovic, M. & Kokotovic, P. V. (2012) *Constructive Nonlinear Control*. Springer Science & Business Media.

Shuai, Z., Sun, Y., Shen, Z. J., Tian, W., Tu, C., Li, Y. & Yin, X. (2016) Microgrid stability: classification and a review. *Renew. Sust. Energ. Rev.*, **58**, 167–179.

Simpson-Porco, J. W., Dörfler, F. & Bullo, F. (2013) Synchronization and power sharing for droop-controlled inverters in islanded microgrids. *Automatica*, **49**, 2603–2611.

Stegink, T., De Persis, C. & van der Schaft, A. (2016) A unifying energy-based approach to stability of power grids with market dynamics. *IEEE Trans. Autom. Control*, **62**, 2612–2622.

Tuffner, F. K., Schneider, K. P., Hansen, J. & Elizondo, M. A. (2018) Modeling load dynamics to support resiliency-based operations in low-inertia microgrids. *IEEE Trans. Smart Grid*, **10**, 2726–2737.

van der Schaft, A. J. & Maschke, B. M. (2013) Port-Hamiltonian systems on graphs. *SIAM J. Control. Optim.*, **51**, 906–937.